LIMNOLOGY and OCEANOGRAPHY

ASLO

Limnol. Oceanogr. 9999, 2023, 1–18

doi: 10.1002/lno.12354

Visual predation risk and spatial distributions of large Arctic copepods along gradients of sea ice and bottom depth

Tom J. Langbehn [1,2*] **Johanna M. Aarflot** [3] **Jennifer J. Freer** [4] **Øystein Varpe** [1,2,5]

[1]Department of Biological Sciences, University of Bergen, Bergen, Norway
[2]Department of Arctic Biology, University Centre in Svalbard, Longyearbyen, Norway
[3]Ecosystem Processes Group, Institute of Marine Research, Bergen, Norway
[4]British Antarctic Survey, Cambridge, UK
[5]Norwegian Institute for Nature Research, Bergen, Norway

Abstract

Changes in the community size structure of Arctic copepods toward smaller and less fat individuals or species have been linked to environmental changes. The underpinning mechanisms are, however, poorly understood. We use a two-step hurdle regression model to analyze spatially resolved, long-term survey data of the Barents Sea mesozooplankton community along gradients of water mass properties, sea ice, and bottom depth. We test the hypothesis that reduced visual predation, and hence increased survival in dim habitats, explains the distribution of large copepods. We expect the presence and biomass of large copepods to increase with increasing bottom depth and the occurrence of seasonal ice-cover. The patterns and drivers that emerge from our analysis support our hypothesis: in the Barents Sea large copepods were predominantly found in deep troughs that intersect the shelf south of the polar front, or at shallower depths in seasonally ice-covered waters northeast of Svalbard. On the banks, large copepods are largely absent whereas smaller copepods appear to survive. Top-down control provides one plausible explanation for these distributions. Large copepods survive where sea-ice shades the water or deep habitats permit escape from visual predators through vertical migrations. However, when upwelled onto shallow banks or flushed out from below the ice they are decimated by visual foragers. Therefore, advection and topographic blockage of vertical zooplankton distributions are key mechanisms for the efficient energy transfer and productivity in subarctic and Arctic shelf seas. New prolific foraging grounds may open up for planktivores where the ice-edge recedes under a changing climate.

Visual foraging is common among planktivorous fishes (Ryer and Olla 1999) and also found in a wide range of other marine planktivores that span several orders of magnitude in size, from small invertebrates, such as amphipods (Kraft et al. 2012) and krill (Torgersen 2001), to seabirds (Stempniewicz et al. 2013), and even baleen whales (Cronin et al. 2017). Many of these planktivores feed on large copepods as their main prey (Huse and Toresen 1996; Karnovsky et al. 2003; Cronin et al. 2017). Globally, the size of marine copepods varies by roughly five orders of magnitude from 10^{-4} to 10^{1} mm, and the largest species are typically found in subpolar and polar oceans (Brun et al. 2016). The large size in polar copepods is often seen as an adaptation to highly seasonal food availability at high latitudes (Scott et al. 2000), where food for pelagic herbivores is only available during the ephemeral spring bloom (Ji et al. 2013). Grazers, such as large copepods of the genus *Calanus*, have adapted to these pulsed environments. They build up lipid reserves to support their winter diapause and reproduction in spring (Falk-Petersen et al. 2009*b*). For visual foragers, copepod size matters; larger individuals and species are often richer in energy-dense lipids (Scott et al. 2000), which means higher energy intake per calorie spent searching and handling prey, and form larger targets more easily spotted than their smaller congenerics (Aksnes and Utne 1997). Therefore, large copepods are an important trophic link in the pelagic, lipid-driven food chain in the Arctic (Falk-Petersen et al. 2009*a*; Record et al. 2018).

The Barents Sea north of Norway and Russia hosts few but abundant planktivorous fish species, the most common ones

*Correspondence: tom.langbehn@uib.no

Additional Supporting Information may be found in the online version of this article.

Author Contribution Statement: T.J.L. and Ø.V. designed the study. J.M.A. contributed the data. T.J.L. analyzed the data with input from J.F. T.J.L wrote the manuscript with contributions from all co-authors. All authors have consented to their authorship and approved the manuscript for publication.

are capelin (*Mallotus villosus*) and Norwegian spring spawning herring (*Clupea harengus*), and further to the north polar cod (*Boreogadus saida*) (Aune et al. 2021). Mature herring feed and overwinter in the Norwegian Sea, but the Barents Sea is an important nursery area for the juvenile part of the population. There are also other zooplanktivores including the juvenile stages of many piscivorous species such as Atlantic cod (*Gadus morhua*), haddock (*Melanogrammus aeglefinus*), saithe (*Pollachius virens*), and beaked redfish (*Sebastes mentella*) (Eriksen et al. 2018). Shallow banks with < 200 m depth allow efficient visual foraging on copepods forced into greater light exposure (Aarflot et al. 2019), and the varied topography of the Barents Sea facilitating both visual foraging and copepod survival, has been suggested as a mechanism contributing to the system's high productivity (Aarflot et al. 2020). Light is key for visual foraging and in addition to the topography, the shading effect of sea ice on the water column presumably structures fish foraging efficiency and consequently the pelagic riskscape for copepods (Langbehn and Varpe 2017). Such strong effects of visual foraging by fish on the zooplankton size structure and community composition are well documented for freshwater systems (Brooks and Dodson 1965).

Climate change has a rapid and unprecedented effect on the Arctic environment, including drastic changes to the underwater light regimes resulting from altered ocean snow and sea-ice cover (Varpe et al. 2015). There is growing concern that increasing temperatures and more open water days due to a shrinking and thinning ice-cover affecting the phenology of the spring bloom may lead to "borealization" or "atlantification" of Arctic marine ecosystems (reviewed in Ingvaldsen et al. 2021) with unknown consequences for its structure and function (Kortsch et al. 2015). Already, community-wide shifts in traits and distribution have been observed. Temperate and boreal demersal fish species in the Barents Sea are extending their distribution northwards in response to increasing temperatures, and have become more dominant at higher latitudes (Fossheim et al. 2015; Frainer et al. 2017). In western Greenland, sea-ice retreat has been linked to shifts towards a smaller and less fat zooplankton species (Møller and Nielsen 2020). These changes may have potentially disruptive effects on the entire food web, in particular when they occur at key lower trophic levels.

Three species of copepods in the genus *Calanus* coexist in the Nordic seas: *Calanus finmarchicus*, *Calanus glacialis*, and *Calanus hyperboreus*; together, they dominate the mesozooplankton biomass in the Barents Sea (Aarflot et al. 2018). They all share a similar morphology and have the same general life cycle but differ notably in their life-history strategies and body size as well as their core distributions (reviewed in Conover 1988 and Daase et al. 2021). The lipid content of *Calanus* spp. scales with body size (Renaud et al. 2018) and the copepodites in developmental stage five of *C. hyperboreus* and *C. glacialis* have 25× and 8× more lipids than *C. finmarchicus*, respectively (Scott et al. 2000). Consequently, trophic transfer efficiency might be reduced in an all-else-equal scenario if the same number of copepods are consumed and the smaller North Atlantic species *C. finmarchicus* replaced its larger Arctic congenerics. In addition, because of differences in annual routines and life histories, that is, capital vs. income breeding, generation time, and timing of diapause (Varpe 2012), shifts in species composition may also affect when energy is transferred to higher trophic levels (Møller and Nielsen 2020).

Capelin provides an illustrative example of how a shift from large Arctic *Calanus* species to their smaller Atlantic congenerics can impact higher trophic levels. Capelin body size and condition have decreased over the past 40 yr off West Greenland and in the Labrador Sea (Renkawitz et al. 2015), coinciding with a shift in hydrographic conditions and a decline in large zooplankton (Mills et al. 2013). Capelin grow faster when feeding on *C. hyperboreus*, rather than *C. finmarchicus* (Hedeholm et al. 2010). This fits well with model predictions for lesser sandeel (*Ammodytes marinus*), another planktivorous fish common in the North Atlantic, which suggests that a reduction in prey size from 2 to 1 mm would roughly halve their energy uptake (van Deurs et al. 2015). In the model, limitations on visual foraging were the most important factor explaining reduced energy uptake. Smaller and less fat capelin as a consequence of smaller and less fat copepods may negatively impact piscivorous predators like Atlantic salmon (*Salmo salar*) (Mills et al. 2013; Renkawitz et al. 2015). Similar effects in response to a shift towards smaller mean copepod size have been predicted for little auks (*Alle alle*) (Stempniewicz et al. 2007), which are the only exclusively zooplanktivorous seabird in the North Atlantic and, with > 100 million individuals, the most abundant seabird species breeding in the Arctic (Barrett et al. 2006).

Because of their central role in polar marine food webs, understanding the mechanisms that govern the distribution of large Arctic copepods is key to make reliable predictions for a future Arctic Ocean. We aim to contribute to a baseline for the distribution of the largest copepods in the Barents Sea and help disentangle the drivers and mechanisms that shape their present and future distributions. We hypothesize that large copepods are more likely to occur and be present in higher numbers, in (i) areas where bottom depth is deep enough for them to migrate vertically to escape predation (sensu Aarflot et al. 2019) or (ii) in areas where sea-ice shading provides relative safety from visual predators even at shallower depth (sensu Langbehn and Varpe 2017). Here, we test these hypotheses by drawing on long term and spatially resolved zooplankton data and sea-ice distributions from the Barents Sea, as well as previous modeling work of prey detection under varying light regimes.

Materials and methods

Biological samples

We analyzed mesozooplankton data from WP2 nets (56 cm diameter, 180 μm mesh size) towed vertically from the seafloor to the surface. All zooplankton samples were collected over a

12-yr period (2008–2020) during the annual Barents Sea Ecosystem Survey (Michalsen et al. 2013; Eriksen et al. 2018) by the Institute of Marine Research (IMR) in late August to September (Fig. 1B).

All zooplankton samples were processed according to the standard IMR sampling procedures (Melle et al. 2004; Skjoldal 2021). In short, each sample is split using a Motoda splitter, one half is preserved in buffered 4% formalin solution for later species identification, and the other half is used for biomass estimates. This latter half is split into fractions of small (180–1000 μm), intermediate (1000–2000 μm), and large (> 2000 μm) body size by successive sieving, starting with the coarsest sieve. Subsequently, the samples were rinsed with freshwater, dried, and weighed for biomass estimates.

Here, we focus on the large (> 2 mm) biomass fraction. Since 2008, macrozooplankton such as amphipods, chaetognaths, krill, fish larvae, and decapod shrimps are routinely hand-picked and removed from the large size fraction. We disregard macrozooplankton in our analysis because they are not representatively sampled by this gear. What is left are largely copepods, typically dominated by adults and late copepodite stages (CV–CVI) of primarily *C. hyperboreus*, but also *Paraeuchaeta* spp. (most likely *Paraeuchaeta norvegica* and *Paraeuchaeta glacialis*), and *C. glacialis*. The smaller *C. finmarchicus* is rarely present in the large size fraction (Skjoldal 2021). Biomass is determined separately for *C. hyperboreus* and *Paraeuchaeta* spp., therefore we assume that the remaining biomass can be largely attributed to *C. glacialis*. Occasionally, smaller individuals that would normally pass through the sieve are retained, but their contribution is small and their effect on the biomass estimates considered negligible (Skjoldal 2021). For a detailed description of the species and stage composition of the three size classes, we refer to Skjoldal (2021, incl. supplementary data).

Environmental data

We focused on four environmental variables in our analysis: bottom depth, sea surface temperature, sea surface salinity, and seasonal sea-ice cover (Fig. 1).

We based bottom depth (Fig. 1A) on the 2021 version of the General Bathymetric Chart of the Oceans (GEBCO Compilation Group 2021) which is available with a 1/4° resolution.

In situ temperature and salinity measurements were available from CTD casts taken alongside the WP2 nets during the surveys (Fig. 1C). We averaged temperature and salinity across the upper 30 m of the water column (Fig. 1D,E) and for the purpose of this study we defined the polar front as the line separating areas where the probability of Atlantic water masses (as defined in Sundfjord et al. 2020) across the 12-yr study period was above or below 50% (Fig. 1F).

We calculated the number of ice-covered days and extracted sea-ice concentrations (Fig. 1G) from daily gridded sea-ice charts produced and made available at a 25 km resolution by the National Snow and Ice Data Centre (Cavalieri et al. 1996). We focus on the week around midsummer because this is when days are longest, and herbivorous copepods are typically in surface waters to graze and reproduce. Consequently, the effect of sea-ice shading is expected to be largest around that time of year. We defined the ice edge as the line north of which the probability of sea-ice covering on average 15% of a given area during the week around midsummer was greater than 50%. We use the same 15% threshold when counting the number of ice-covered days per year.

Preparation of survey data for statistical modeling

Sampling effort and exact location of the survey stations varied across years, in the northeast of the study area in particular, due to weather, seasonal ice cover or limited survey time. Therefore, we aggregated all samples and environmental data on a 35 × 35 nautical mile (1 nm = 1.852 km) grid using the Albers equal-area projection (Fig. 1B,C; *see* Supporting Information Fig. S1 for exact parameter settings). In years with more than one sampling station per grid cell, and for bottom depth and sea-ice concentrations, we used grid cell averages. We only considered complete net casts that covered the full water column, that is, from within 30 m of the seafloor to the surface. We also omitted cells where either zooplankton data, or any of the environmental variables were missing, and we constrained our analysis to the shelf region with bottom depth less than 500 m (Fig. 1A). Furthermore, we excluded grid cells that were surveyed infrequently (< 4 times out of the 12 study years). In total, this left 1953 WP2 nets (and associated CTD casts) from 160 stations. With this selection, 95% of the stations were sampled in at least 6 different years (Supporting Information Fig. S2).

Predictors

We assessed multicollinearity among candidate environmental predictors using the variance inflation factor. From our initial set of five environmental predictors, temperature and the number of ice-covered days per year were most strongly correlated (Pearson's correlation coefficient, $r = -0.85$, $p < 0.001$). After removing ice-covered days from the list of environmental predictors, the variance inflation factor for all remaining covariates was less than three, which is an acceptable threshold suggested by Zuur et al. (2010). The remaining four environmental predictors, among which sea ice and bottom depth were the least correlated ($r = -0.30$, $p < 0.001$), were included in the models.

Statistical approach

Initial data exploration revealed that the zooplankton biomass for the large size fraction was zero-inflated and overdispersed (Supporting Information Fig. S3), which is common in ecological data but needs to be accounted for when modeling abundance. Therefore, we used a hurdle model approach in which the probability of occurrence, and abundance or

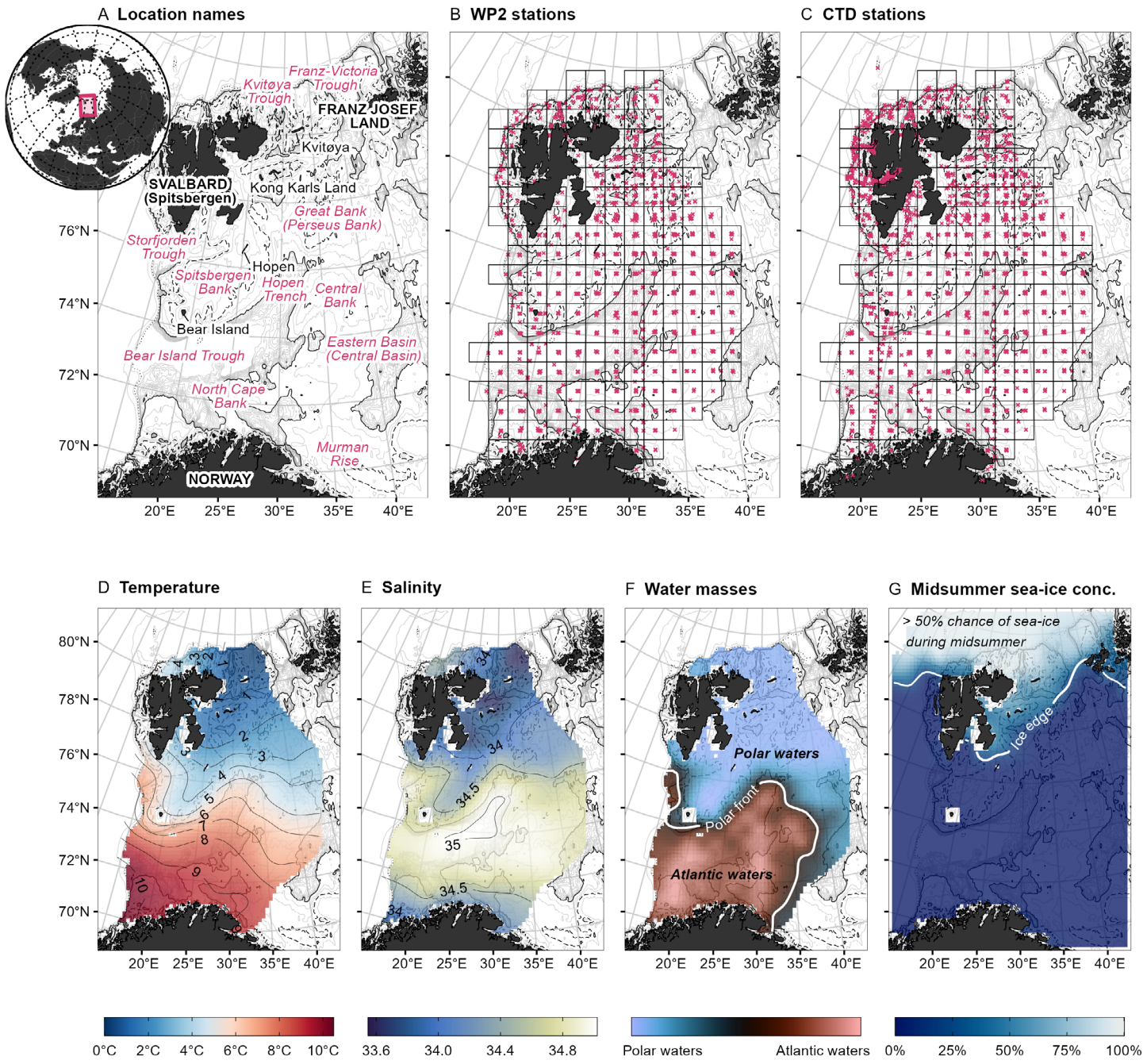

Fig. 1. Maps of the study area showing (**A**) location names referenced throughout the text and bottom topography (--- 150 m, — 300 m, ··· 500 m), bottom topography is further shown in all maps; (**B**,**C**) the WP2 and CTD survey stations for the years 2008–2020 considered in this study, overlaid by a 35 × 35 nautical mile (1 nm = 1.852 km) sampling grid; (**D**,**E**) temperature (°C) and salinity(PSU) at sampling averaged across the top 30 m of the water column; (**F**) water mass distributions, and **(G)** sea-ice concentrations during midsummer. North of the ice-edge, the likelihood of at least 15% sea-ice cover during midsummer is larger than 50%. All panels show the median values for the study period from 2008 to 2020.

biomass conditional on presence are modeled in a two-step process from the same data (Zuur et al. 2009).

Hurdle models are frequently used to model species distributions (Langton et al. 2021). A benefit of this approach is that it acknowledges the possibility that mechanisms that control species presence are different, or may act on different scales, from those controlling species abundance. For example, the method allows for stochastic processes that may lead to a site being unoccupied despite being suitable (Tyre et al. 2001).

Here, we fit hurdle models to the combined large copepod fraction, as well as to the three subsets; C. *hyperboreus* only,

Paraeuchaeta spp. only, and the remaining unidentified fraction (presumed to be mainly *C. glacialis*).

Model fitting and selection

First, we modeled the probability of occurrence of large copepods in a given environment ("the hurdle") using a binomial generalized additive model (GAM) with a logit link function fitted to binary presence-absence data. All stations with positive biomass were classed as present and assigned the value one, while station where large copepods were absent were assigned zeros. Then, in the second step, we predicted large copepod biomass using a GAM with Tweedie distribution and the default log-link fitted to the presence-only data (i.e., sites that "cleared the hurdle").

Full models (before model selection) for both the binomial and Tweedie GAM were of the following form:

$$g(n_{x,y}) = \mathrm{te}(x,y) + s_1\left(\mathrm{depth}_{x,y}\right) + s_2\left(\mathrm{temp}_{x,y}\right) + s_3\left(\mathrm{sal}_{x,y}\right) + s_4\left(\mathrm{ice}_{x,y}\right) + \mathrm{ti}\left(\mathrm{depth}_{x,y}, \mathrm{ice}_{x,y}\right)$$

where n is either the probability of occurrence when the response is binary (i.e., presence–absence), or estimated biomass in case of presence-only data; g is the link between n and the additive predictors; te is tensor smooth of geographical position (x, y), s_1 to s_4 are cubic spline smooth functions of bottom depth (*depth*), temperature (*temp*), salinity (*sal*), midsummer sea-ice concentration (*ice*), and ti is a tensor smooth function (allowing for different scales or units) of the interaction between bottom depth and sea ice. We included Northings and Eastings (x, y) as terms to explicitly account for spatial autocorrelation in the model (Wood 2017). We estimated the splines with the restricted maximum likelihood optimization method and applied an additional null space penalization which allowed for the complete removal of a covariate when the smoothing was equal to zero (Marra and Wood 2011). We limited the number of knots for the univariate smoothing terms to 3 and 4 for the binomial GAM and Tweedie GAM respectively, to avoid overfitting. All GAMs were fitted using the *mgcv* library in R (Wood 2017; Supporting Information Figs. S4, S5).

We removed nonsignificant predictors using a backwards selection approach based on Akaike's information criteria (AIC). The predictor with highest nonsignificant (> 0.05) p-value was dropped from the model, provided it also decreased the AIC; or if the difference in AIC was less than two, the model with fewest covariates was kept. Smooths that were penalized to zero were also removed from the final model. Note that because the hurdle model approach allows different processes and drivers to govern species presence and biomass, the set of predictors in the two stages of the hurdle model do not necessarily have to be the same (Zuur et al. 2009).

We compared model fitted values against observations using a Taylor Diagram (Supporting Information Fig. S6). Finally, predictions for the probability of occurrence and the estimated biomass, as well as their product, which can be interpreted as the biomass weighted by the probability of occurrence, were projected onto an 8.75×8.75 nautical mile ($\sim 16 \times 16$ km) grid to visually assess the model performance against the survey data (Supporting Information Fig. S7).

All analyses were done in R 4.1.1 (R Core Team 2021), and we refer to the session info provided at the end source code for a complete list of all loaded packages and version numbers.

Results

Spatial distribution

Copepods in the large size fraction were not uniformly distributed across the western Barents Sea. Two areas with similarly high median biomass stand out: (i) the deep troughs in the Barents Sea Opening south of the polar front where bottom depths exceed 300 m (mean $\pm$ SD $= 360 \pm 46$ m), and (ii) the region northeast of Svalbard which is shallower (180 ± 40 m; Supporting Information Table S1) but remains largely ice-covered ($59\% \pm 24\%$) during the height of the summer (Fig. 2A). In both areas, average median biomass was around 0.26–0.33 g dry mass (DM) m^{-2}. Biomass was generally lowest around the banks (i.e., Spitsbergen Bank, Central Bank and Great Bank). On the banks, in more years than not, no large copepods were caught in the WP2 nets at the majority of the stations.

This bimodal distribution pattern of high biomass was to some extent driven by the contrasting distributions of two key taxa: *Paraeuchaeta* spp. in the Barents Sea Opening to the south (Fig. 2B) and *C. hyperboreus* in ice-covered waters to the northeast (Fig. 2C; Supporting Information Fig. S9). When averaged across stations, these two taxa account for around 50% of the large copepod biomass in the WP2 samples.

Paraeuchaeta spp. was found almost exclusively south of the polar front in the Bear Island Trough and Hopen Trench and predominantly in deep waters with bottom depth > 300 m (Fig. 2B; Supporting Information Fig. S9). In deep waters south of the polar front, *Paraeuchaeta* spp. was the single most important taxa and accounted for more than half of the average median biomass ($63\% \pm 32\%$; Supporting Information Table S3) with values of 0.096 ± 0.058 g DM m^{-2} (Supporting Information Table S4).

However, average median biomass was reduced by three quarters to 0.026 ± 0.027 g DM m^{-2} (Supporting Information Table S4) for stations with bottom depth < 300 m. Beyond the ice-edge the contribution of *Paraeuchaeta* spp. was negligible, and with an average median biomass of 0.0022 ± 0.0075 g DM m^{-2}, made up less than 1% of the total biomass in the large size fraction.

In contrast, *C. hyperboreus* was distributed mostly in waters north of the summer ice-edge, around Kvitøya, where sea-ice lasts for more than 220 ± 27 d each year

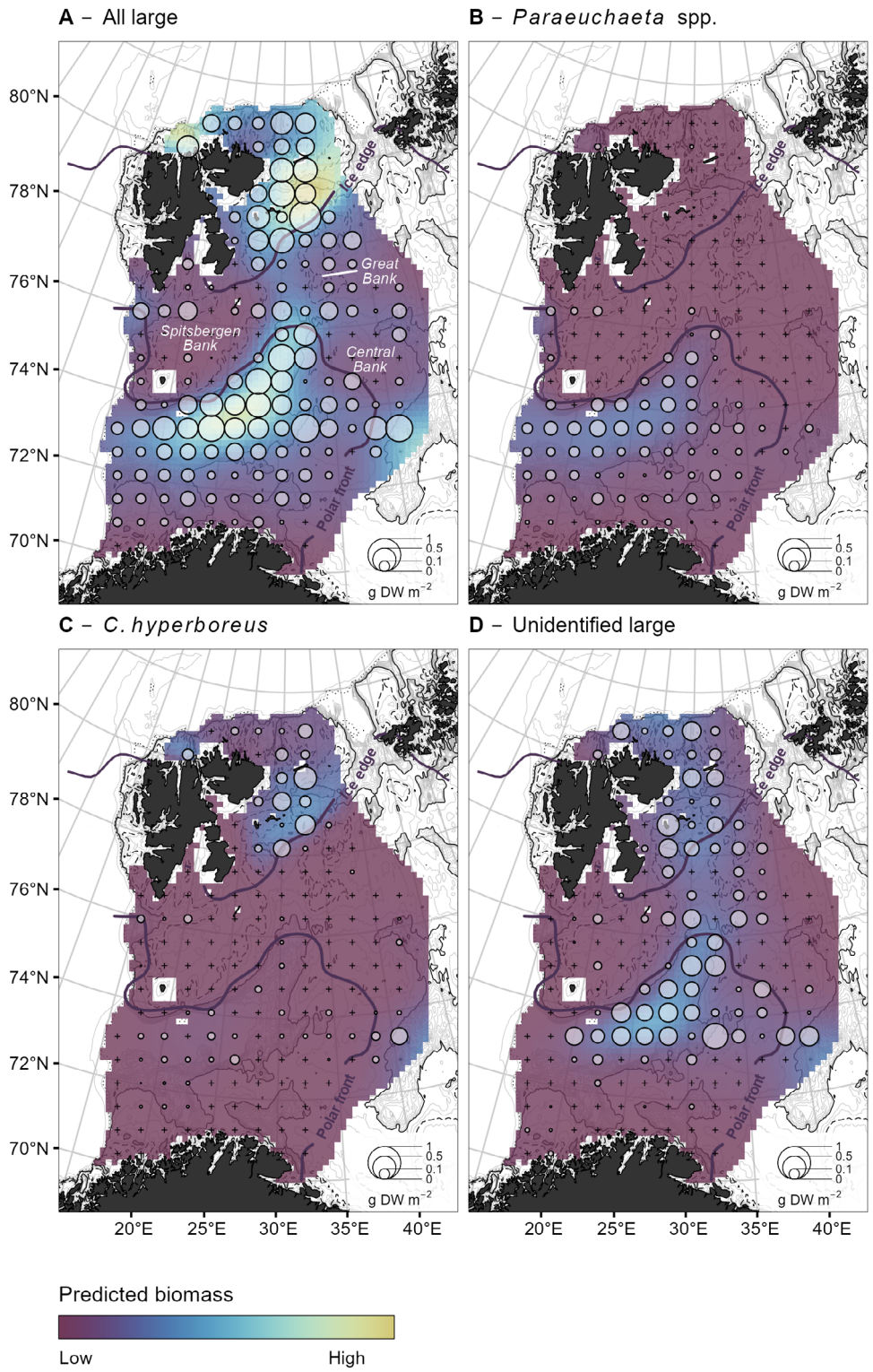

Fig. 2. Observed and predicted biomass distribution of large copepods (> 2 mm) in the western Barents Sea; (**A**) pooled, or split into (**B**) *Paraeuchaeta* spp., (**C**) *Calanus hyperboreus*, and (**D**) the remaining unidentified fraction. Size of the dots indicates the observed median biomass (g DM m^{-2}) within a given grid cell for samples taken between 2008 and 2020. Crosses indicate that in more years than not, no large copepods were sampled at a given station. Background colors indicate the biomass weighted by the probability of occurrence as predicted by the hurdle model. The midsummer ice-extent (> 50% chance of at least 15% sea-ice cover during the week around midsummer) and the polar front are marked by dark blue lines for spatial reference.

(Fig. 2C; Supporting Information Table S1). North of the ice-edge *C. hyperboreus* contributes 33% ± 30% of the large copepod biomass (average across stations) with an average median biomass of 0.1 ± 0.13 g DM m^{-2}. The species is also regularly found in the deep troughs to the south, but at much lower abundances. At stations south of the polar front and with bottom depth > 300 m, the average median biomass of *C. hyperboreus* was an order of magnitude lower than in the north with only 0.013 ± 0.017 g DM m^{-2}. For stations where *C. hyperboreus* was present in more years than not, the minimum depth of occurrence was 40 m shallower in ice-covered waters when compared to ice-free waters (Supporting Information Fig. S9).

The average median biomass both for *Paraeuchaeta* spp. and *C. hyperboreus* was lowest on the banks (bottom depth < 200 m) between the polar front and the summer ice-edge, with 0.0023 ± 0.013 and 0.0033 ± 0.012 g DM m^{-2} (Supporting Information Table S2), for the two species, respectively. In most years, however, neither species was caught across the majority of the stations located on the banks (indicated by crosses in Fig. 2).

The remaining fraction of large unidentified copepods, most likely later developmental stages of *C. glacialis*, had similar patterns. Stations with consistently high biomass were located in the eastern part of the deeper Bear Island Trough and Hopen Trench and north of the summer ice-edge. The Spitsbergen and Central banks were areas of low biomass. However, the unidentified fraction accounted for almost the entire biomass in the largest size fraction around the Great Bank, just south of the ice-edge (Fig. 2D).

Hurdle model evaluation

The comparison of the observed vs. the predicted biomass, both for combined and individual taxa, suggests a good model fit (Supporting Information Fig. S6; Fig. 2). The models reliably predicted areas of high and low biomass and successfully captured less prominent patterns seen in the observations such as the influx of *Paraeuchaeta* spp. through the Storfjorden Trough around 76°N (Fig. 2B), or the high biomass of *C. hyperboreus* in the Eastern Basin at latitudes far south of the ice-edge (Fig. 2C).

Table 1. Model statistics for the binomial and Tweedie GAM fitted to the combined large size fraction (all large), *Calanus hyperboreus*, *Paraeuchaeta* spp., and the remaining unidentified fraction. Model statistics are presented for each individual smoother term. Statistics indicate chi-square (binomial) and *F* (Tweedie) test statistics for assessing the significance of model smooth terms; *p*-values indicate approximate *p*-values for the null hypotheses that each smooth term is zero.

	Model	Dev. expl. (%)	R^2 adj.	Term	Edf	Statistics	*p*-value
Binomial GAM	All large	38.5	0.31	te(*X*, *Y*)	8.34	17.7	< 0.05
				s(depth)	1.42	13.8	< 0.001
	Paraeuchaeta spp.	69.1	0.74	*s*(depth)	0.94	13.6	< 0.001
				s(temp)	1.53	18.8	< 0.001
				s(sal)	0.91	9.5	< 0.001
				s(ice)	1.01	10.1	< 0.001
	C. hyperboreus	53.7	0.56	te(*X*, *Y*)	9.24	31.6	< 0.001
				s(depth)	1.77	12.3	< 0.001
				s(temp)	0.69	1.9	< 0.05
				s(ice)	0.80	2.1	< 0.05
				ti(depth, ice)	3.14	10.4	< 0.01
	Remaining large	36.7	0.37	te(*X*, *Y*)	11.00	36.1	< 0.001
				s(depth)	0.92	10.7	< 0.001
				s(ice)	0.82	3.2	< 0.05
Tweedie GAM	All large	65.2	0.64	te(*X*, *Y*)	10.60	3.16	< 0.001
				s(depth)	0.98	14.90	< 0.001
				s(temp)	0.92	3.93	< 0.001
				s(ice)	1.28	4.02	< 0.001
	Paraeuchaeta spp.	63.7	0.67	*s*(depth)	2.58	22.80	< 0.001
				s(sal)	0.93	4.51	< 0.001
	C. hyperboreus	58.5	0.33	te(*X*, *Y*)	5.48	1.06	< 0.001
				s(depth)	0.80	1.37	< 0.05
				s(ice)	1.61	3.96	< 0.01
	Remaining large	43.3	0.30	te(*X*, *Y*)	5.51	2.29	< 0.001
				s(depth)	2.14	10.30	< 0.001
				s(ice)	0.77	1.13	< 0.05

Dev. expl., deviance explained; Edf, estimated degrees of freedom; R^2 adj., adjusted coefficient of determination; Term, model smooth terms.

After model selection, the binomial GAMs explained a medium to high percentage of the deviance in presence–absence data. The explained deviance was similar for the combined large fraction and the remaining unidentified fraction with 38.5% and 36.3%, respectively. The model for *Paraeuchaeta* spp. explained 69.1% and the model for *C. hyperboreus* 53.7% (Table 1). The deviance explained by the Tweedie GAM fitted to the presence only data was 65.2% for the combined large fraction, 63.7% for *Paraeuchaeta* spp., 58.5% for *C. hyperboreus*, and 43.3% for the remaining unidentified fraction (Table 1).

Drivers of the distribution

The presence of *Paraeuchaeta* spp. was best predicted by a model that included bottom depth, temperature, salinity, and midsummer sea-ice concentrations (Table 1).

Paraeuchaeta spp. was increasingly likely to occur in deeper, warmer, and more saline Atlantic water masses. At bottom depth $\gtrsim$ 280 m and temperatures and salinities above 7.5°C and 34.7 psu, the probability of occurrence was more than 50% (Fig. 3A–C). The species was predicted to be likely absent at bottom depth < 200 m and at temperatures < 4.5°C. Sea ice had an additional positive effect on the probability of occurrence at intermediate ($\sim$ 20–85%) summer sea-ice concentrations (Fig. 3D).

Bottom depth and salinity were significant predictors for the biomass of *Paraeuchaeta* spp. (Table 1). We predict higher than average densities of *Paraeuchaeta* spp. at a depth of $\gtrsim$ 350 m (Fig. 3E) and a salinity of $\gtrsim$ 34.8 psu (Fig. 3F).

The presence–absence of *C. hyperboreus* was best predicted by a model including bottom depth, temperature, salinity, and the interaction between midsummer sea-ice concentration and bottom depth, as well as the geographical position (Table 1).

The model predicts a sigmoid relationship between the presence of *C. hyperboreus* and bottom depth. In shallow areas the species was more likely to be absent, but the probability of occurrence increased rapidly between 150 and 300 m bottom

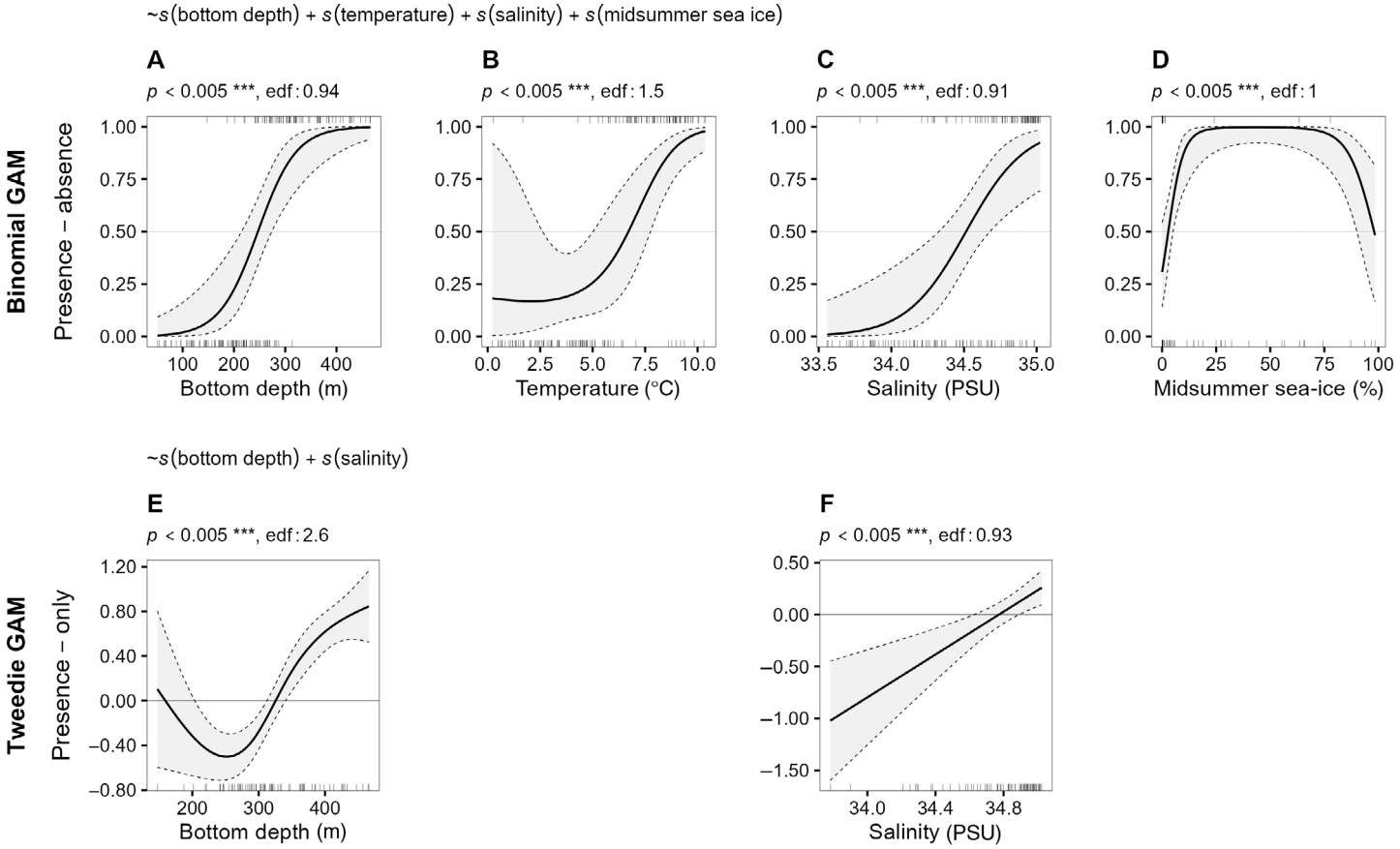

Fig. 3. Partial effects of key environmental factors on the probability of species presence (top row, **A**–**D**) and biomass conditional on presence (bottom row, **E**,**F**) of *Paraeuchaeta* spp. in the western Barents Sea. Each panel shows the shape of response for one environmental variable independent of the other variables. Solid lines and shaded areas show the mean and 95% confidence intervals. The distribution of samples is given by the rugs on the *x*-axis. Confidence intervals are calculated to include the uncertainty about the overall mean. Significance levels and estimated degrees of freedom are indicated on top of each panel. Only significant terms included in the most parsimonious model, as indicated on top of each row, are shown. Note that the *y*-axis in the plots for the binomial GAM (top row) shows the probability of occurrence, while for the Tweedie GAM (bottom row) values on the *y*-axis represent the deviation from the mean predicted biomass on the scale of the predictor, that is, a change of 0.5 on the log link scale used here would suggest a 65% increase in biomass.

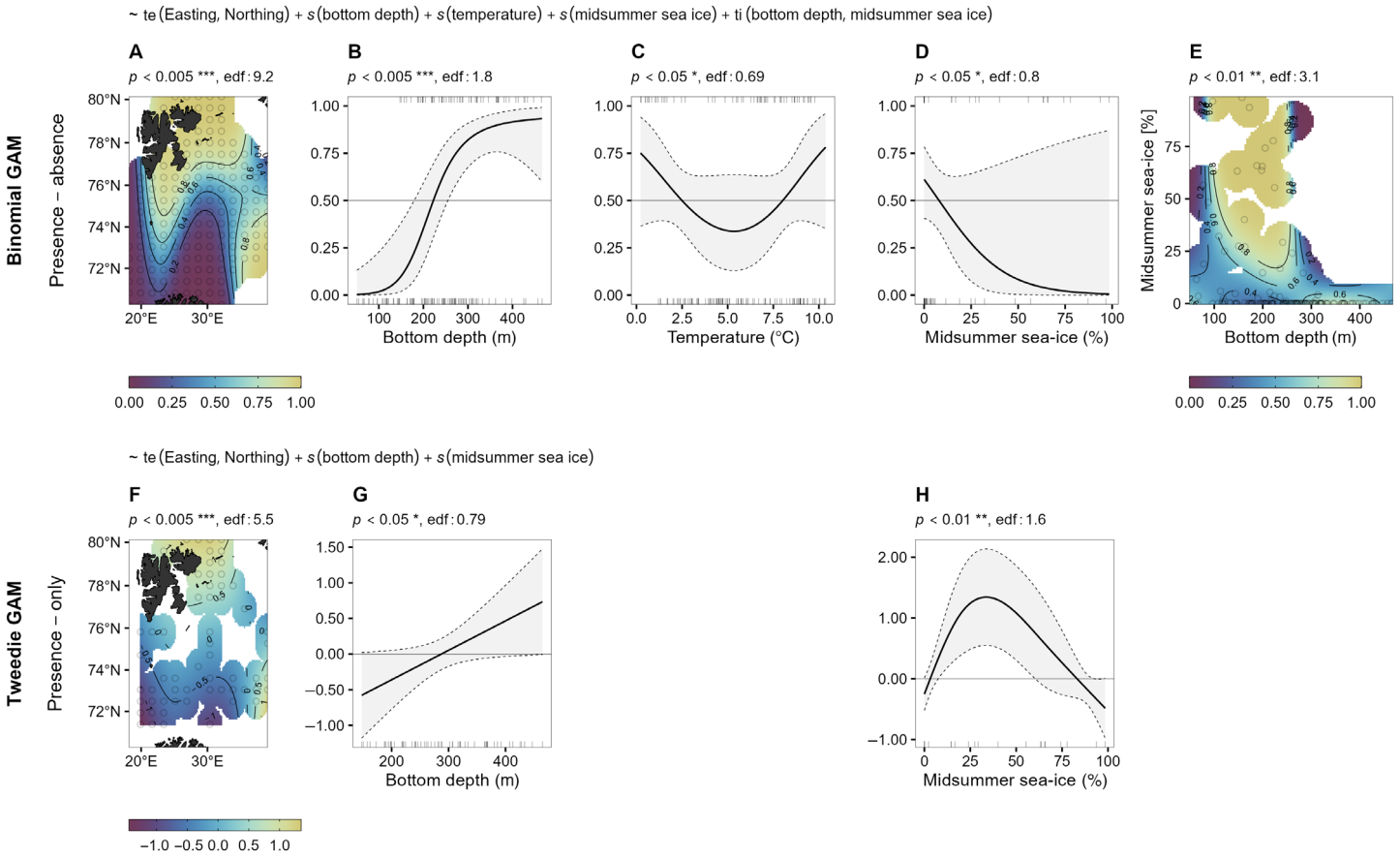

Fig. 4. Partial effects of key environmental factors on the probability of species presence (top row, **A**–**E**) and biomass conditional of presence (bottom row, **F**–**H**) of *Calanus hyperboreus* in the western Barents Sea. Line plots shows the shape of the response for one environmental variable independent of the other variables, with solid lines and shaded areas indicating the mean and 95% confidence intervals. The distribution of samples is given by the rugs on the *x*-axis. Confidence intervals are calculated to include the uncertainty about the overall mean. Contour plots show interactions with darker colors indicating lower and lighter colors higher values. Only significant terms included in the most parsimonious model, as indicated on top of each row, are shown. Note that the *y*-axis in the plots for the binomial GAM (top row) shows the probability of occurrence, while for the Tweedie GAM (bottom row) values on the *y*-axis represent the deviation from the mean predicted biomass on the scale of the predictor, that is, a change of 0.5 on the log link scale used here would suggest a 65% increase in biomass.

depth, with > 50% probability of occurrence at > 260 m bottom depth (Fig. 4B).

C. *hyperboreus* was least likely to occur at temperatures between ~ 2.5°C and 7.5°C, and more likely to be found at either the cold or warm end of the temperature gradient (Fig. 4C). The partial effect of sea ice was predicted to be negative. However, although significant, the partial effects of sea-ice concentration and temperature on the occurrence of *C. hyperboreus* are inconclusive as the confidence intervals overlapped across the entire range of values. But there was a significant interaction between sea ice and bottom depth. *C. hyperboreus* was more likely to occur in shallow areas (shallower than predicted based on bottom depth alone, see Fig. 4B) when sea ice was present (Fig. 4E). This effect increased with increasing sea-ice concentrations up to 50% sea-ice cover. The spatial interaction term suggested a higher probability of occurrence of *C.hyperboreus* north of the polar front (Fig. 4A), implying that spatial variance was linked to some water mass properties other than temperature or salinity, for example, advection or food availability.

Bottom depth, midsummer sea-ice concentrations, and geographical position were significant predictors for the biomass of *C. hyperboreus* (Table 1). The biomass of *C. hyperboreus* was predicted to be above average where midsummer sea-ice concentration was between approximately 10–60%, with a broad peak around 35% (Fig. 4H). Furthermore, *C. hyperboreus* biomass was positively, linearly related to depth (Fig. 4G), and higher than average values were found northeast of Svalbard, and in the Eastern Basin (Fig. 4F).

The presence and abundance of the remaining large fraction, presumably largely *C. glacialis*, appears to be linked to the same environmental drivers as *Paraeuchaeta* spp. and

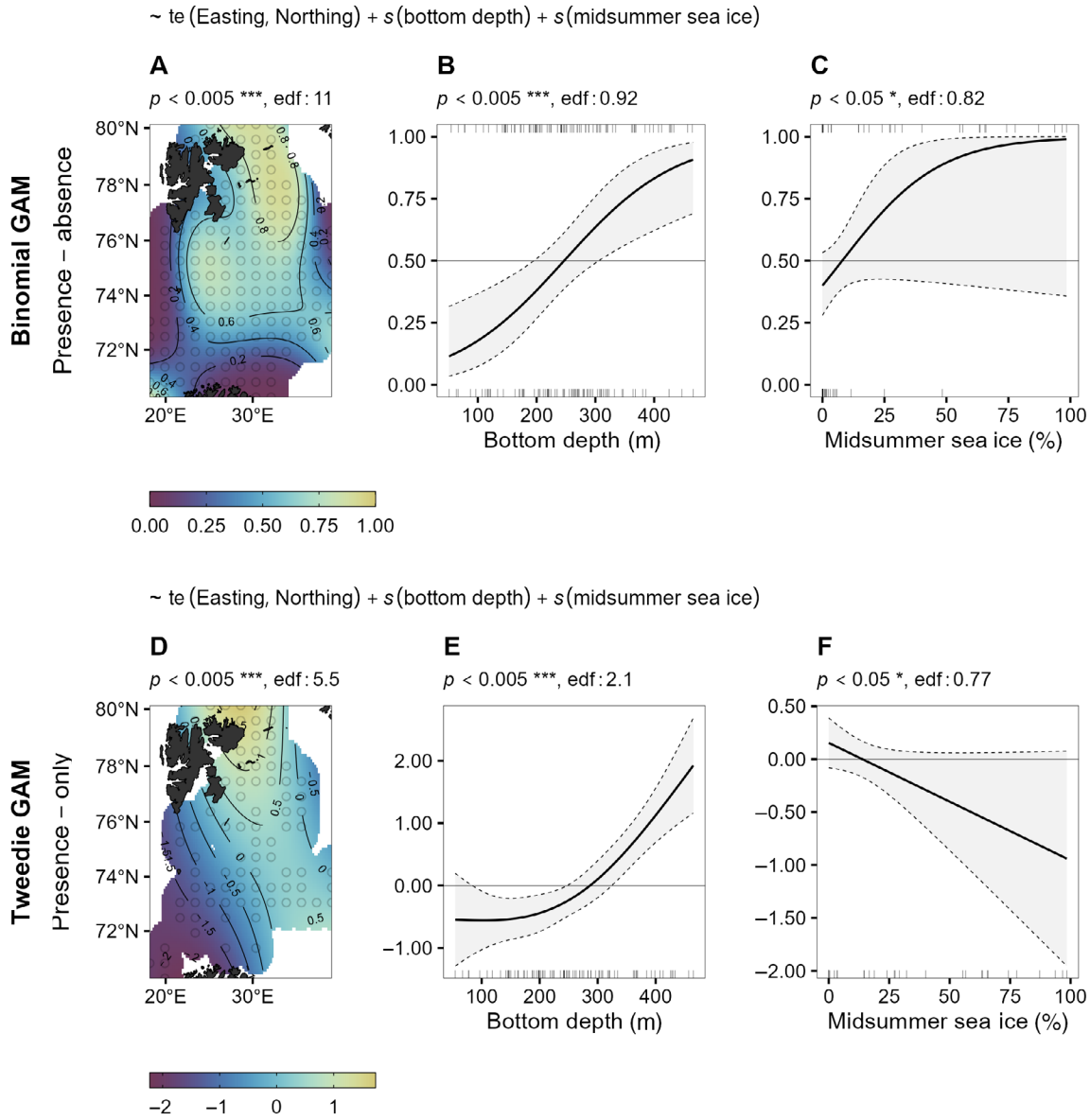

Fig. 5. Partial effects of key environmental factors on the probability of species presence (top row, **A**–**C**) and biomass conditional on presence (bottom row, **D**–**F**) of the remaining unidentified copepods in the large size fraction from the western Barents Sea, after *Paraeuchaeta* spp. and *Calanus hyperboreus* had been removed. Line plots show the shape of the response for one environmental variable independent of the other variables, with solid lines and shaded areas indicating the mean and 95% confidence intervals. The distribution of samples is given by the rugs on the *x*-axis. Confidence intervals are calculated to include the uncertainty about the overall mean. Contour plots show interactions with darker colors indicating lower and lighter colors higher values. Only significant terms included in the most parsimonious model, as indicated on top of each row, are shown. Note, that the *y*-axis in the plots for the binomial GAM (top row) shows the probability of occurrence, while for the Tweedie GAM (bottom row) values on the *y*-axis represent the deviation from the mean predicted biomass on the scale of the predictor, that is, a change of 0.5 on the log link scale used here would suggest a 65% increase in biomass.

C. hyperboreus, namely bottom depth and seasonal ice-cover (Table 1). The model predicts the probability of occurrence (Fig. 5B) and the abundance (Fig. 5E) to increase with increasing bottom depth. The species was most likely present and predicted to occur with higher-than-average biomass at bottom depth $\gtrsim$ 250 m. Midsummer sea-ice cover was positively related to the probability of occurrence (Fig. 5C) and negatively related to biomass (Fig. 5F). However, variability was large and the confidence intervals for sea-ice overlap across the full range of possible values. Hence the partial effect of sea ice should be interpreted with caution. An additional term for spatial interaction suggests that unidentified large copepods were more likely found in the center and in the north of the study area but were less likely to be present at the

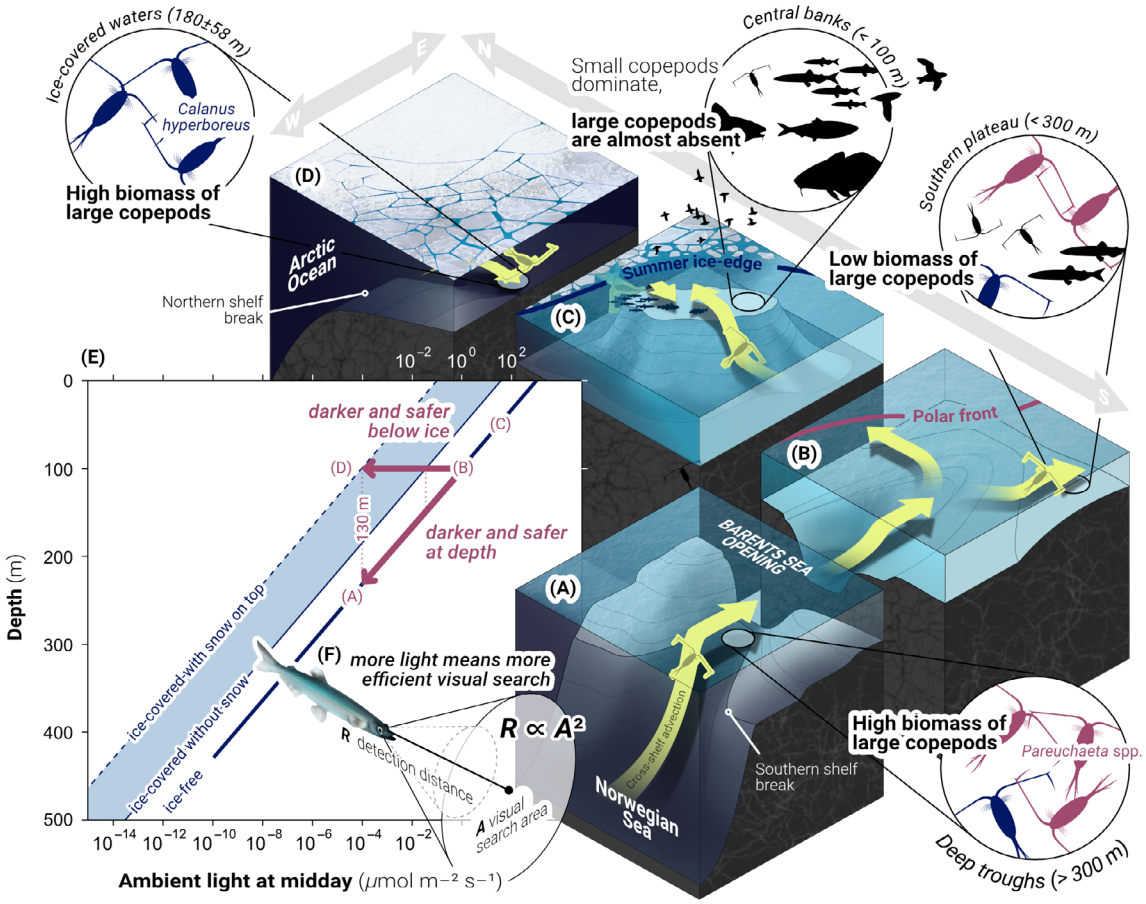

Fig. 6. Conceptual visualization of the key mechanism shaping the distribution of large copepods in the Barents Sea. (**A**) Large copepods are transported onto the Barents Sea shelf with Atlantic water masses through the Barents Sea Opening in the southwest. (**B**) Their downward migration becomes blocked in shallow waters by the seafloor, and they are exposed to light intensities several orders of magnitudes brighter than their usual light environment. (**C**) Large copepods are almost absent on the sun-lit banks, likely because they are quickly decimated by visual predators, such as fish and zooplanktivorous seabirds. This explains why the shallow banks are foraging hotspots and among the areas with the highest biological activity in the Barents Sea. (**D**) In the northern Barents Sea, sea-ice shading creates refugia with dim light where large copepods advected onto the shelf from the north are relatively safe from visual predation. (**E**) Below sea ice, the light environment is similar to that at much greater depth in ice-free waters. The light conditions over depth are shown for relatively clear water (diffuse attenuation coefficient of 0.07 m^{-1}, Aarflot et al. 2020) and 1-m-thick sea ice, either with or without 30 cm of fresh snow on top (King et al. 2017). We assume albedo values of 0.05 for open water, 0.5 for bare ice and 0.9 for snow-covered ice, and attenuation coefficients of 20 m^{-1} for snow, 5 m^{-1} for the upper 10 cm of ice, and 1 m^{-1} for the ice interior (Perovich 1996). (**F**) The search efficiency of visual predators' scales with ambient light. At the ice-edge large copepods are flushed out into the light which makes the marginal ice-zone an attractive place for visual foragers. The combination of shallow waters and a receding ice-edge could make the Arctic shelf seas future foraging hotspots.

western, southern, and eastern margins of the region (Fig. 5A). The biomass of these copepods was predicted to gradually increase from the southwest toward the northeast (Fig. 5D).

Significant predictors for the combined large size fraction were bottom depth for the probability of occurrence, and bottom depth, sea ice, and temperature for total biomass (Table 1). These predictions agree with the taxa-specific models. The binomial GAM predicts a sigmoidal relationship for species presence with bottom depth, similar to those seen in all other three models (Supporting Information Fig. S8B). Furthermore, abundance is predicted to be linearly related to bottom depth and temperature (Supporting Information Fig. S8D,E), with higher-than-average biomass predicted at depths > 270 m and > 5.5°C. The predicted relationship between biomass and sea ice is dome-shaped, with peak biomass predicted around 45% midsummer sea-ice cover (Supporting Information Fig. S8F).

Discussion

In the Barents Sea, *C. hyperboreus* was most abundant in cold, low-salinity, relatively shallow but ice-covered waters, and only occurred sporadically south of the polar front in the deepest troughs. This contrasts the distribution of *Paraeuchaeta* spp. which was almost exclusively found south of the polar front in warm, saline, deep and ice-free waters.

The herbivorous *C. hyperboreus* is commonly considered an Arctic oceanic species, that has its core distribution in the deep basins of the Greenland Sea and Arctic Ocean (Falk-Petersen et al. 2009*b*; Aarflot et al. 2022). *Paraeuchaeta* spp., on the other hand, are carnivorous deep-water species that feed on other copepods, with at least 10 different species known to occur in the subarctic North Atlantic (Park 1994). All of them, except *P. polaris* which is endemic to the Arctic Ocean, are typically associated with Atlantic water masses. Hence, superficially, the observed distributions in the Barents Sea may appear unsurprising as both key taxa are associated with the same water masses as elsewhere. However, this does not explain why both species are practically absent on the shallow banks in the Barents Sea, and why *C. hyperboreus* are found much shallower in ice-covered waters than in ice-free waters south of the ice-edge. Scrutinizing the potential mechanisms that could lead to these patterns reveals a common, plausible explanation: in both cases, large copepods are more abundant in dim environments associated with reduced risk of visual predation.

Although the biology of *C. hyperboreus* and *Paraeuchaeta* spp. is different, they are both associated with deep habitats, at least for parts of the year. *Paraeuchaeta* spp. are quasi permanent residents of the dysphotic mesopelagic zone (200–1000 m). In *P. norvegica*, ovigerous females and individuals with large energy reserves, both of which are particular conspicuous to visual predators, were found to have deeper distributions than the rest of the population, presumably to avoid predation (Vestheim 2004). Although some species in the genus are known to perform diel vertical migrations (Yen 1985), they typically avoided the upper waters, even at night (Bollens and Frost 1991; Fleddum et al. 2001). *C. hyperboreus*, in contrast, performs extensive seasonal vertical migrations and overwinters in diapause at several hundred meters depth at times when food near the surface is scarce in these high latitude environments (Falk-Petersen et al. 2009*b*). Because both species rely on deep habitats it seems reasonable to assume that these strategies have evolved outside of the Barents Sea, suggesting their presence in this shallow shelf sea system is likely the result of expatriation through advection.

We found that *Paraeuchaeta* spp. in the Barents Sea were almost entirely restricted to Atlantic water masses, and predominantly found in the deep trough systems in the Barents Sea Opening, while being essentially absent in shallower locations. Predictions from a coupled particle tracking and production model have shown a very similar distribution for mesozooplankton that are advected with Atlantic Water from the Greenland Sea and Norwegian Sea in to the Barents Sea (see Fig. 3 in Wassmann et al. 2019 in comparison to Fig. 2 in this study). Water exchange across the Barents Sea Opening varies between seasons and years but the net inflow is around 2–3 Sv (1 Sverdrup = 10^6 m^3 s^{-1}) with velocities of up to 20 cm s^{-1} (Edvardsen et al. 2003; Smedsrud et al. 2022). The strong currents in the area, together with the observed distribution suggest that *Paraeuchaeta* spp. are upwelled from their usual North-Atlantic deep-water habitat and flushed into the Barents Sea by cross-shelf advection through the troughs that intersect the western shelf break (Fig. 6A). Individuals that are transported further into the Barents Sea with the currents are likely to sooner or later end up on the banks where they become trapped by shallow bottom topography (Fig. 6B,C). On the banks, daytime light intensities are several orders of magnitudes higher than in their typical deep-water habitat (Fig. 6E). More light means higher foraging efficiency for visual predators (Fig. 6F) such as planktivorous fish (Aksnes and Utne 1997), and large zooplankton are particularly vulnerable to visual predation as they are more easily spotted than smaller prey items (O'Brien 1979). Following such a top-down logic, rather than a bottom-up argument where low abundance indicates poor feeding conditions and an unfavorable environment for copepods, their near absence on the banks could be explained by efficient fish foraging and thus energy transfer to higher trophic levels. Atlantic water masses from the southwest and polar waters from the northeast could provide a supply of large, energy rich prey that when advected onto the banks, where they are exposed to higher than usual light intensities, become available to visual predators and are quickly decimated. During their annual feeding migration, capelin form fronts that sweep across the Barents Sea (Fauchald et al. 2006) and can locally deplete mesozooplankton biomass in a matter of 3–4 d (Hassel et al. 1991). Furthermore, continuous zooplankton scattering layers often show gaping holes downstream of banks, presumably as a result of efficient predation on the banks where the vertical migration of organisms forming these layers gets blocked by the seafloor (Genin et al. 1988, 1994) or lakebed (Houghton et al. 2010). The same mechanism has been proposed for subsea canyons or shelf breaks where entire predator assemblages line the edges waiting for prey to arrive in the form of vertical migrators caught outside their light comfort zone (Pereyra et al. 1969). Foraging aggregations over shallow topographies may attract larger predators that profit from the same mechanisms of topographic blockage. In the Barents Sea, cod (*Gadus morhua*) benefit from capelin coming near the seafloor (Fall et al. 2021), and studies from Newfoundland show that cod have a higher amount of capelin in stomach samples from shallower areas (Fahrig et al. 1993). Shallow banks in the northern Barents Sea are also central foraging grounds for cetaceans feeding on capelin and other prey (Skern-Mauritzen et al. 2011). Therefore, topographic blockage at least partly explains why productive fisheries are often concentrated on or near banks or abrupt rises in bottom topography. Heightened productivity over abrupt topographies may also be caused by upwelling of nutrients and the associated increased primary production (Genin 2004; Falk-Petersen et al. 2015).

The topographic blockage mechanism was introduced by Isaacs and Schwartzlose (1965) and its importance for the vertical distribution of Barents Sea zooplankton and fish foraging efficiency has been previously described in detail by Aarflot

et al. (2019, 2020). Our study on an independent dataset supports their findings and corroborates the importance of bottom depth as a key factor structuring pelagic communities through changes in foraging interaction strength. In this study, bottom depth was the only environmental variable retained for all GAMs fitted. In most cases, the partial effects of bottom depth showed a sigmoidal response of presence–absence and/or biomass over depth (e.g., Fig. 3A or 4B). Prey detection distance of visual foragers over depth would have the same shape, just mirrored, with larger detection distances closer to the surface and a rapid decline as light decreases exponentially with depth (visualized in Aarflot et al. 2020). This substantiates a causal link between bottom depth and visual foraging as the effect of trapping and concentrating zooplankton would rapidly lose its importance at depth where light is too faint for visual foragers—whose eyes are adapted to light intensities near the surface—to detect their prey.

Although topographic blockage provides a parsimonious explanation to the observed distribution of *Paraeuchaeta* spp. in the Barents Sea, at first, it seems to fit less well for *C. hyperboreus*. This species occurred in low numbers in the deeper areas south of the polar front (a distribution similar to that of *Paraeuchaeta* spp. in the area) but was most abundant in the ice-covered regions northeast of Svalbard. Here, the average bottom depth is much shallower (180 ± 40 m; Supporting Information Table S1) than in the troughs to the south (360 ± 46 m; Supporting Information Table S1), yet *C. hyperboreus* appears to thrive despite what the topographic blockage mechanism would suggest. We found that the interaction between sea ice and bottom depth was a significant predictor for its distribution. Both the data (Supporting Information Fig. S8) and the model (Fig. 4D) suggest that *C. hyperboreus* was more likely to be present at shallow bottom depth (< 200 m) in seasonally ice-covered waters. Herring and capelin in the Barents Sea are mostly in the upper part of the water column (Huse and Toresen 1996) and models suggest that these planktivorous fishes are most efficient in the upper 150 m and unlikely to visually detect copepods at depth greater than 200 m in the Barents Sea (Aarflot et al. 2019). Several smaller troughs intersect the steep shelf break to the northeast of Svalbard and are the main gateways through which polar waters flow south onto the shelf. One could expect large copepods to be most abundant where they are first upwelled and their biomass to gradually decline further away from the shelf-break as the chance of being eaten by visual predators increases with time. Such a gradual decline can be seen, for example, southeast of the Bear Island Trough where the abundance of *Paraeuchaeta* spp. progressively decreases away from the shelf break and decreasing bottom depth. However, what we see for *C. hyperboreus* is an abrupt drop in biomass across the marginal ice zone several hundred kilometers south of the northern shelf-break. Sea ice, especially when thick and snow-covered, is extremely efficient in blocking light from reaching the waters below (Perovich 1996, Fig. 6E), making it difficult for visual predators to detect their prey (Langbehn and Varpe 2017). In consequence, the higher-than-average abundances of *C. hyperboreus* in sea-ice-covered waters, might be explained by the addition of sea-ice shading (Fig. 6D) that creates a light environment similar to that found at much greater depth in ice-free waters (Fig. 6E). Model predictions for the northern Barents Sea suggest that a shift towards ice-free conditions could boost visual foraging efficiency of planktivores by as much as 16-fold (Langbehn and Varpe 2017). Vilgrain et al. (2021) documented a similar size gradient with larger copepods below the ice, and smaller copepods in ice-free open waters across the marginal ice-zone in Baffin Bay, Canada. In their case, there was no significance difference in the abundance and species composition of adult individuals across the ice-edge, whereas young copepod stages from all *Calanus* species were much more abundant in the ice-free eastern part. Therefore, they concluded that the size gradient was more likely caused by high recruitment of young copepod stages in response to sea-ice melt and increased primary production, than size differences between advected Atlantic and Arctic communities. However, this cannot explain the observed differences across the marginal ice zone in the Barents Sea, because we only analyzed the largest size fraction, which typically does not contain juvenile stages. Nonetheless, recruitment and high abundances of juvenile stages in ice-free waters may add to the size gradient during other times of the annual cycle. In conclusion, visual foraging (although enacted through different mechanisms, i.e., topographic blockage vs. sea-ice shading) can provide a unified explanation for the occurrence of *Paraeuchaeta* spp. and *C. hyperboreus* across different water masses and temperature regimes in the Barents Sea, and plausibly explains the general absence of large copepods from the banks. Our interpretation is consistent with findings from previous studies that show that the growth of polar cod (*Boreogadus saida*) and the biomass of capelin is higher in the Barents Sea in years with less sea ice and an earlier breakup, while the biomass of copepods typically decreased in those years (Stige et al. 2019; Dupont et al. 2020). In years when the ice-edge is far north, the center of the capelin distribution is also further north, following the receding ice-edge (Orlova et al. 2010; Ingvaldsen and Gjøsæter 2013). In the time around 1690–1790, during the peak of European whaling, the ice-edge was as far as 82° north, far off the shelf, and strong northeasterly winds resulted in pronounced upwelling along the shelf. This upwelling may have brought large copepods onto the shelf and fueled high primary and secondary production, likely sustaining the historically large abundances of whales north of Svalbard (Falk-Petersen et al. 2015). With the ice-extent dwindling in the Arctic, a prediction that follows from our analysis is that the shallow areas around Kvitøya and along the northern shelf break in the Barents Sea may become foraging hotspots for visually searching planktivores, and because of size-selective predation, may result in a shift towards smaller mean

copepod size. This prediction appears to be supported by observations from Disko Bay in Western Greenland where fewer ice-covered days and more open water have been linked to the increased dominance of smaller and less fat zooplankton species with more Atlantic affinities (Møller and Nielsen 2020). There, *C. finmarchicus* has now largely replaced the larger Arctic congenerics, but the challenge remains to disentangle the contribution of increased top-down control in ice-free waters from the change of water masses. Similar trends have also been observed for the Barents Sea. The biomass of *C. finmarchicus* has increased since around 2005, while that of *C. glacialis* in the Barents Sea Opening is trending downwards (Aarflot et al. 2018), at the same time as an increased inflow of warmer Atlantic water and a decrease in sea ice (Efstathiou et al. 2022).

However, while a decline in sea ice and mean copepod size in the western Greenland Sea may have resulted in poorer feeding conditions for capelin (Renkawitz et al. 2015), this may not necessarily be the case for the northern Barents Sea in an ice-free future. Our analysis suggests that large copepods in the Barents Sea are most likely expatriate populations that are sustained by source-sink-dynamics through advection from core populations in the deeper basins of the adjacent Nordic Seas and central Arctic Ocean. Consequently, in an all-else equal scenario, increased predation in the Barents Sea is unlikely to affect core parts of these populations. Therefore, a boost in visual search as sea-ice retreats may benefit planktivores and increase stock productivity in the northern Barents Sea as prey accessibility increases.

A second line of evidence emerges from the freshwater literature. The introduction of planktivorous fish into once fishless lakes strongly affects the biomass, community composition, size structure, and life-history traits of lower trophic level zooplankton, with cascading effects to phytoplankton production. Typically, the change in predation regime leads to a decline in abundance of large-bodied zooplankton individuals or species, while favoring smaller, less conspicuous forms (Brooks and Dodson 1965; Schabetsberger et al. 2009) with shorter life histories, for example, smaller size at first reproduction (Wathne et al. 2020). Several studies have corroborated these observations and, as the ultimate test of causality, demonstrated that recovery to predisturbance levels after fish removal is possible (Knapp et al. 2001). Studies have also shown that following severely cold winters the mean zooplankton body size in lakes was significantly larger in the following summer (Isermann et al. 2004; Jackson et al. 2007; Balayla et al. 2010). The suggested mechanism is that oxygen depletion under ice, particularly in shallow lakes, lead to severe fish mortality and hence a predatory release of larger zooplankton in the following year. Reduced visual foraging efficiency under ice (Langbehn and Varpe 2017) is an alternative, nonmutually exclusive explanation for the increased zooplankton body size after severe ice winters. Mesocosm studies with experimentally controlled light regimes have shown that fish predation leads to smaller than average body size and lower zooplankton biomass; however, the effect diminished with declining light levels (Bramm et al. 2009). Similarly, brownification as the result of increasing input of humic substances reduces light availability in aquatic ecosystems and has been shown (in an experimental pond system) to increase winter mortality in fish due to decreased search efficiency and consequently increased starvation (Hedström et al. 2017). Accordingly, in lakes that are ice-covered for most parts of the year, encounters below the ice might be too rare to sustain planktivores or prevent them from building up sufficient surplus energy for successful reproduction in the following year (Shuter et al. 2012) explaining reduced fish abundance after severe winters.

Concluding remarks

Species distribution modeling is frequently based on fixed and assumed correlations between environmental factors and observed patterns of distribution and abundance. However, interpretation and predictive capabilities are limited when the underpinning mechanisms are unknown. Here, we propose that size-selective predation by visual foragers provides a parsimonious and mechanistic explanation for the spatial distribution of large copepods in the Barents Sea and argue that advection, sea-ice shading, and topographic blockage play a key role. This case study exemplifies how several environmental drivers can contribute through different processes to the same overarching mechanism. Finally, this work suggests that part of the production harvested within the Barents Sea likely originates hundreds and thousands of kilometers downstream in the Norwegian and Greenland Seas. This production is then advected into the Barents Sea, neatly packaged as large copepods, where it then becomes available for planktivores and ultimately higher-level predators. These linkages have implications for the spatial scales of ecosystem-based management.

Data availability statement

The data that support the findings of this study are openly available in the following repositories: Bathymetry and sea-ice data were retrieved from the General Bathymetric Chart of the Oceans (GEBCO Compilation Group 2021) and the National Snow and Ice Data Centre (Cavalieri et al. 1996). Zooplankton as well as temperature and salinity data from the Barents Sea Ecosystem Survey are available through the Norwegian Marine Data Centre (NMDC) at https://nmdc.no/. For convenience, we additionally provide the annotated source and all data needed to run the analysis in the supporting information.

References

Aarflot, J. M., H. R. Skjoldal, P. Dalpadado, and M. Skern-Mauritzen. 2018. Contribution of *Calanus* species to the mesozooplankton biomass in the Barents Sea. ICES J. Mar. Sci. **75**: 2342–2354. doi:10.1093/icesjms/fsx221

Aarflot, J. M., D. L. Aksnes, A. F. Opdal, H. R. Skjoldal, and Ø. Fiksen. 2019. Caught in broad daylight: Topographic constraints of zooplankton depth distributions. Limnol. Oceanogr. **64**: 849–859. doi:10.1002/lno.11079

Aarflot, J. M., P. Dalpadado, and Ø. Fiksen. 2020. Foraging success in planktivorous fish increases with topographic blockage of prey distributions. Mar. Ecol. Prog. Ser. **644**: 129–142. doi:10.3354/meps13343

Aarflot, J. M., S. S. Hjøllo, E. Strand, and M. D. Skogen. 2022. Transportation and predation control structures the distribution of a key calanoid in the Nordic Seas. Prog. Oceanogr. **202**: 102761. doi:10.1016/j.pocean.2022.102761

Aksnes, D. L., and A. C. W. Utne. 1997. A revised model of visual range in fish. Sarsia **82**: 137–147. doi:10.1080/00364827.1997.10413647

Aune, M., and others. 2021. Distribution and ecology of polar cod (*Boreogadus saida*) in the eastern Barents Sea: A review of historical literature. Mar. Environ. Res. **166**: 105262. doi:10.1016/j.marenvres.2021.105262

Balayla, D., T. L. Lauridsen, M. Søndergaard, and E. Jeppesen. 2010. Larger zooplankton in Danish lakes after cold winters: Are winter fish kills of importance? Hydrobiologia **646**: 159–172. doi:10.1007/s10750-010-0164-4

Barrett, R. T., G. Chapdelaine, T. Anker-Nilssen, A. Mosbech, W. A. Montevecchi, J. B. Reid, and R. R. Veit. 2006. Seabird numbers and prey consumption in the North Atlantic. ICES J. Mar. Sci. **63**: 1145–1158. doi:10.1016/j.icesjms.2006.04.004

Bollens, S. M., and B. W. Frost. 1991. Ovigerity, selective predation, and variable diel vertical migration in *Euchaeta elongata* (Copepoda: Calanoida). Oecologia **87**: 155–161. doi:10.1007/BF00325252

Bramm, M. E., M. K. Lassen, L. Liboriussen, K. Richardson, M. Ventura, and E. Jeppesen. 2009. The role of light for fish-zooplankton-phytoplankton interactions during winter in shallow lakes—A climate change perspective. Freshw. Biol. **54**: 1093–1109. doi:10.1111/j.1365-2427.2008.02156.x

Brooks, J. L., and S. I. Dodson. 1965. Predation, body size, and composition of plankton. Science **150**: 28–35. doi:10.1126/science.150.3692.28

Brun, P., M. R. Payne, and T. Kiørboe. 2016. Trait biogeography of marine copepods—An analysis across scales. Ecol. Lett. **19**: 1403–1413. doi:10.1111/ele.12688

Cavalieri, D. J., C. L. Parkinson, P. Gloersen, and H. J. Zwally. 1996. Sea ice concentrations from Nimbus-7 SMMR and DMSP SSM/I-SSMIS passive microwave data, version 1 [daily, Arctic Ocean, 2008–2020]. doi:10.5067/8GQ8LZQVL0VL

Conover, R. J. 1988. Comparative life histories in the genera *Calanus* and *Neocalanus* in high latitudes of the northern hemisphere. Hydrobiologia **167–168**: 127–142. doi:10.1007/BF00026299

Cronin, T. W., J. I. Fasick, L. E. Schweikert, S. Johnsen, L. J. Kezmoh, and M. F. Baumgartner. 2017. Coping with copepods: Do right whales (*Eubalaena glacialis*) forage visually in dark waters? Philos. Trans. R. Soc. Lond. B Biol. Sci. **372**: 20160067. doi:10.1098/rstb.2016.0067

Daase, M., J. Berge, J. E. Søreide, and S. Falk-Petersen. 2021. Ecology of Arctic pelagic communities, p. 219–259. *In* D. N. Thomas [ed.], Arctic ecology. Wiley.

Dupont, N., J. M. Durant, Ø. Langangen, H. Gjøsæter, and L. C. Stige. 2020. Sea ice, temperature, and prey effects on annual variations in mean lengths of a key Arctic fish, *Boreogadus saida*, in the Barents Sea. ICES J. Mar. Sci. **77**: 1796–1805. doi:10.1093/icesjms/fsaa040

Edvardsen, A., D. Slagstad, K. S. Tande, and P. Jaccard. 2003. Assessing zooplankton advection in the Barents Sea using underway measurements and modelling. Fish. Oceanogr. **12**: 61–74. doi:10.1046/j.1365-2419.2003.00219.x

Efstathiou, E., T. Eldevik, M. Årthun, and S. Lind. 2022. Spatial patterns, mechanisms, and predictability of Barents Sea ice change. J. Climate **35**: 2961–2973. doi:10.1175/JCLI-D-21-0044.1

Eriksen, E., and others. 2018. From single species surveys towards monitoring of the Barents Sea ecosystem. Prog. Oceanogr. **166**: 4–14. doi:10.1016/j.pocean.2017.09.007

Fahrig, L., G. R. Lilly, and D. S. Miller. 1993. Predator stomachs as sampling tools for prey distribution: Atlantic Cod (*Gadus morhua*) and capelin (*Mallotus villosus*). Can. J. Fish. Aquat. Sci. **50**: 1541–1547. doi:10.1139/f93-175

Falk-Petersen, S., T. Haug, H. Hop, K. T. Nilssen, and A. Wold. 2009*a*. Transfer of lipids from plankton to blubber of harp and hooded seals off East Greenland. Deep-Sea Res. II Top. Stud. Oceanogr. **56**: 2080–2086. doi:10.1016/j.dsr2.2008.11.020

Falk-Petersen, S., P. Mayzaud, G. Kattner, and J. R. Sargent. 2009*b*. Lipids and life strategy of Arctic *Calanus*. Mar. Biol. Res. **5**: 18–39. doi:10.1080/17451000802512267

Falk-Petersen, S., V. Pavlov, J. Berge, F. Cottier, K. M. Kovacs, and C. Lydersen. 2015. At the rainbow's end: High productivity fueled by winter upwelling along an Arctic shelf. Polar Biol. **38**: 5–11. doi:10.1007/s00300-014-1482-1

Fall, J., E. Johannesen, G. Englund, G. O. Johansen, and Ø. Fiksen. 2021. Predator–prey overlap in three dimensions: Cod benefit from capelin coming near the seafloor. Ecography **44**: 802–815. doi:10.1111/ecog.05473

Fauchald, P., M. Mauritzen, and H. Gjøsæter. 2006. Density-dependent migratory waves in the marine pelagic ecosystem. Ecology **87**: 2915–2924 doi:10.1890/0012-9658(2006)87[2915:DMWITM]2.0.CO;2.

Fleddum, A., S. Kaartvedt, and B. Ellertsen. 2001. Distribution and feeding of the carnivorous copepod *Paraeuchaeta norvegica* in habitats of shallow prey assemblages and midnight sun. Mar. Biol. **139**: 719–726. doi:10.1007/s002270100618

Fossheim, M., R. Primicerio, E. Johannesen, R. B. Ingvaldsen, M. M. Aschan, and A. V. Dolgov. 2015. Recent warming leads to a rapid borealization of fish communities in the Arctic. Nat. Clim. Change **5**: 673–677. doi:10.1038/nclimate2647

Frainer, A., R. Primicerio, S. Kortsch, M. Aune, A. V. Dolgov, M. Fossheim, and M. M. Aschan. 2017. Climate-driven changes in functional biogeography of Arctic marine fish communities. Proc. Natl. Acad. Sci. U.S.A. **114**: 12202–12207. doi:10.1073/pnas.1706080114

GEBCO Compilation Group. 2021. GEBCO 2021 grid. doi:10.5285/c6612cbe-50b3-0cff-e053-6c86abc09f8f

Genin, A. 2004. Bio-physical coupling in the formation of zooplankton and fish aggregations over abrupt topographies. J. Mar. Syst. **50**: 3–20. doi:10.1016/j.jmarsys.2003.10.008

Genin, A., L. Haury, and P. Greenblatt. 1988. Interactions of migrating zooplankton with shallow topography: Predation by rockfishes and intensification of patchiness. Deep Sea Res. A Oceanogr. Res. Pap. **35**: 151–175. doi:10.1016/0198-0149(88)90034-9

Genin, A., and others. 1994. Zooplankton patch dynamics: Daily gap formation over abrupt topography. Deep-Sea Res. I Oceanogr. Res. Pap. **41**: 941–951. doi:10.1016/0967-0637(94)90085-X

Hassel, A., H. R. Skjoldal, H. Gjøsæter, H. Loeng, and L. Omli. 1991. Impact of grazing from capelin (Mallotus villosus) on zooplankton: a case study in the northern Barents Sea in August 1985. Polar Research **10**: 371–388. doi:10.1111/j.1751-8369.1991.tb00660.x

Hedeholm, R., P. Grønkjær, A. Rosing-Asvid, and S. Rysgaard. 2010. Variation in size and growth of West Greenland capelin (*Mallotus villosus*) along latitudinal gradients. ICES J. Mar. Sci. **67**: 1128–1137. doi:10.1093/icesjms/fsq024

Hedström, P., D. Bystedt, J. Karlsson, F. Bokma, and P. Byström. 2017. Brownification increases winter mortality in fish. Oecologia **183**: 587–595. doi:10.1007/s00442-016-3779-y

Houghton, C., C. Bronte, R. Paddock, and J. Janssen. 2010. Evidence for allochthonous prey delivery to lake Michigan's mid-lake reef complex: Are deep reefs analogs to oceanic sea mounts? J. Great Lakes Res. **36**: 666–673. doi:10.1016/j.jglr.2010.07.003

Huse, G., and R. Toresen. 1996. A comparative study of the feeding habits of herring (*Clupea harengus*, Clupeidae, L.) and capelin (*Mallotus villosus*, Osmeridae, Müller) in the Barents Sea. Sarsia **81**: 143–153. doi:10.1080/00364827.1996.10413618

Ingvaldsen, R. B., and H. Gjøsæter. 2013. Responses in spatial distribution of Barents Sea capelin to changes in stock size, ocean temperature and ice cover. Mar. Biol. Res. **9**: 867–877. doi:10.1080/17451000.2013.775450

Ingvaldsen, R. B., K. M. Assmann, R. Primicerio, M. Fossheim, I. V. Polyakov, and A. V. Dolgov. 2021. Physical manifestations and ecological implications of Arctic Atlantification. Nat. Rev. Earth Environ. **2**: 874–889. doi:10.1038/s43017-021-00228-x

Isaacs, J. D., and R. A. Schwartzlose. 1965. Migrant sound scatterers: Interaction with the sea floor. Science **150**: 1810–1813. doi:10.1126/science.150.3705.1810

Isermann, D. A., S. R. Chipps, and M. L. Brown. 2004. Seasonal *Daphnia* biomass in winterkill and nonwinterkill glacial lakes of South Dakota. N. Am. J. Fish. Manag. **24**: 287–292. doi:10.1577/M02-151

Jackson, L. J., T. L. Lauridsen, M. Søndergaard, and E. Jeppesen. 2007. A comparison of shallow Danish and Canadian lakes and implications of climate change. Freshw. Biol. **52**: 1782–1792. doi:10.1111/j.1365-2427.2007.01809.x

Ji, R., M. Jin, and Ø. Varpe. 2013. Sea ice phenology and timing of primary production pulses in the Arctic Ocean. Glob. Change Biol. **19**: 734–741. doi:10.1111/gcb.12074

Karnovsky, N., S. Kwasniewski, J. Weslawski, W. Walkusz, and A. Beszczynska-Möller. 2003. Foraging behavior of little auks in a heterogeneous environment. Mar. Ecol. Prog. Ser. **253**: 289–303. doi:10.3354/meps253289

King, J., G. Spreen, S. Gerland, C. Haas, S. Hendricks, L. Kaleschke, and C. Wang. 2017. Sea-ice thickness from field measurements in the northwestern Barents Sea. J. Geophys. Res. Oceans **122**: 1497–1512. doi:10.1002/2016JC012199

Knapp, R. A., K. R. Matthews, and O. Sarnelle. 2001. Resistance and resilience of alpine lake fauna to fish introductions. Ecol. Monogr. **71**: 401–421 doi:10.1890/0012-9615(2001)071[0401:RAROAL]2.0.CO;2.

Kortsch, S., R. Primicerio, M. Fossheim, A. V. Dolgov, and M. Aschan. 2015. Climate change alters the structure of arctic marine food webs due to poleward shifts of boreal generalists. Proc. R. Soc. B Biol. Sci. **282**: 20151546. doi:10.1098/rspb.2015.1546

Kraft, A., J. Berge, Ø. Varpe, and S. Falk-Pedersen. 2012. Feeding in Arctic darkness: Mid-winter diet of the pelagic amphipods *Themisto abyssorum* and *T. libellula*. Mar. Biol. **160**: 241–248. doi:10.1007/s00227-012-2065-8

Langbehn, T. J., and Ø. Varpe. 2017. Sea-ice loss boosts visual search: Fish foraging and changing pelagic interactions in polar oceans. Glob. Chang. Biol. **23**: 5318–5330. doi:10.1111/gcb.13797

Langton, R., P. Boulcott, and P. Wright. 2021. A verified distribution model for the lesser sandeel *Ammodytes marinus*. Mar. Ecol. Prog. Ser. **667**: 145–159. doi:10.3354/meps13693

Marra, G., and S. N. Wood. 2011. Practical variable selection for generalized additive models. Comput. Stat. Data Anal. **55**: 2372–2387. doi:10.1016/j.csda.2011.02.004

Melle, W., B. Ellertsen, and H. Skjoldal. 2004. Zooplankton: The link to higher trophic levels, p. 137–202. *In* H. Skjoldal [ed.], The Norwegian Sea ecosystem. Tapir Academic Press.

Michalsen, K., and others. 2013. Marine living resources of the Barents Sea—Ecosystem understanding and monitoring in a climate change perspective. Mar. Biol. Res. **9**: 932–947. doi:10.1080/17451000.2013.775459

Mills, K. E., A. J. Pershing, T. F. Sheehan, and D. Mountain. 2013. Climate and ecosystem linkages explain widespread declines in North American Atlantic salmon populations. Glob. Chang. Biol. **19**: 3046–3061. doi:10.1111/gcb.12298

Møller, E. F., and T. G. Nielsen. 2020. Borealization of Arctic zooplankton—Smaller and less fat zooplankton species in Disko Bay, Western Greenland. Limnol. Oceanogr. **65**: 1175–1188. doi:10.1002/lno.11380

O'Brien, W. J. 1979. The predator–prey interaction of planktivorous fish and zooplankton: Recent research with planktivorous fish and their zooplankton prey shows the evolutionary thrust and parry of the predator–prey relationship. Am. Sci. **67**: 572–581.

Orlova, E., G. Rudneva, P. Renaud, K. Elane, P. Todd, V. Savinov, and A. Yurko. 2010. Climate impacts on feeding and condition of capelin *Mallotus villosus* in the Barents Sea: Evidence and mechanisms from a 30 year data set. Aquat. Biol. **10**: 105–118. doi:10.3354/ab00265

Park, T. 1994. Geographic distribution of the bathypelagic genus *Paraeuchaeta* (Copepoda, Calanoida). Hydrobiologia **292–293**: 317–332. doi:10.1007/BF00229957

Pereyra, W. T., F. E. C. Jr, and W. G. Pearcy. 1969. *Sebastodes flavidus*, a shelf rockfish feeding on mesopelagic fauna, with consideration of the ecological implications. J. Fish. Board Can. **26**: 2211–2214. doi:10.1139/f69-205

Perovich, D. K. 1996. The optical properties of sea ice. 96–1. US Army Corps of Engineers Cold Regions Research & Engineering Laboratory.

Record, N. R., R. Ji, F. Maps, Ø. Varpe, J. A. Runge, C. M. Petrik, and D. Johns. 2018. Copepod diapause and the biogeography of the marine lipidscape. J. Biogeogr. **45**: 2238–2251. doi:10.1111/jbi.13414

Renaud, P. E., and others. 2018. Pelagic food-webs in a changing Arctic: A trait-based perspective suggests a mode of resilience. ICES J. Mar. Sci. **75**: 1871–1881. doi:10.1093/icesjms/fsy063

Renkawitz, M., T. Sheehan, H. Dixon, and R. Nygaard. 2015. Changing trophic structure and energy dynamics in the Northwest Atlantic: Implications for Atlantic salmon feeding at West Greenland. Mar. Ecol. Prog. Ser. **538**: 197–211. doi:10.3354/meps11470

Ryer, C., and B. Olla. 1999. Light-induced changes in the prey consumption and behavior of two juvenile planktivorous fish. Mar. Ecol. Prog. Ser. **181**: 41–51. doi:10.3354/meps181041

Schabetsberger, R., M. S. Luger, G. Drozdowski, and A. Jagsch. 2009. Only the small survive: Monitoring long-term changes in the zooplankton community of an Alpine lake after fish introduction. Biol. Invasions **11**: 1335–1345. doi:10.1007/s10530-008-9341-z

Scott, C. L., S. Kwasniewski, S. Falk-Petersen, and J. R. Sargent. 2000. Lipids and life strategies of *Calanus finmarchicus*, *Calanus glacialis* and *Calanus hyperboreus* in late autumn, Kongsfjorden, Svalbard. Polar Biol. **23**: 510–516. doi:10.1007/s003000000114

Shuter, B. J., A. G. Finstad, I. P. Helland, I. Zweimüller, and F. Hölker. 2012. The role of winter phenology in shaping the ecology of freshwater fish and their sensitivities to climate change. Aquat. Sci. **74**: 637–657. doi:10.1007/s00027-012-0274-3

Skern-Mauritzen, M., E. Johannesen, A. Bjørge, and N. Øien. 2011. Baleen whale distributions and prey associations in the Barents Sea. Mar. Ecol. Prog. Ser. **426**: 289–301. doi:10.3354/meps09027

Skjoldal, H. R. 2021. Species composition of three size fractions of zooplankton used in routine monitoring of the Barents Sea ecosystem. J. Plankton Res. **43**: 762–772. doi:10.1093/plankt/fbab056

Smedsrud, L. H., and others. 2022. Nordic seas heat loss, Atlantic inflow, and Arctic Sea ice cover over the last century. Rev. Geophys. **60**: e2020RG000725. doi:10.1029/2020RG000725

Stempniewicz, L., K. Błachowiak-Samołyk, and J. M. Węsławski. 2007. Impact of climate change on zooplankton communities, seabird populations and arctic terrestrial ecosystem—A scenario. Deep-Sea Res. II Top. Stud. Oceanogr. **54**: 2934–2945. doi:10.1016/j.dsr2.2007.08.012

Stempniewicz, L., and others. 2013. Visual prey availability and distribution of foraging little auks (*Alle alle*) in the shelf waters of West Spitsbergen. Polar Biol. **36**: 949–955. doi:10.1007/s00300-013-1318-4

Stige, L. C., E. Eriksen, P. Dalpadado, and K. Ono. 2019. Direct and indirect effects of sea ice cover on major zooplankton groups and planktivorous fishes in the Barents Sea. ICES J. Mar. Sci. **76**: i24–i36. doi:10.1093/icesjms/fsz063

Sundfjord, A., K. M. Assmann, Ø. Lundesgaard, A. H. H. Renner, S. Lind, and R. B. Ingvaldsen. 2020. Suggested water mass definitions for the central and northern Barents Sea, and the adjacent Nansen Basin. Nansen Legacy Rep. Ser. doi:10.7557/nlrs.5707

Torgersen, T. 2001. Visual predation by the euphausiid *Meganyctiphanes norvegica*. Mar. Ecol. Prog. Ser. **209**: 295–299. doi:10.3354/meps209295

Tyre, A. J., H. P. Possingham, and D. B. Lindenmayer. 2001. Inferring process from pattern: Can territory occupancy provide information about life history parameters? Ecol. Appl. **11**: 1722–1737 doi:10.1890/1051-0761(2001)011[1722:IPFPCT]2.0.CO;2.

van Deurs, M., C. Jørgensen, and Ø. Fiksen. 2015. Effects of copepod size on fish growth: A model based on data for North Sea sandeel. Mar. Ecol. Prog. Ser. **520**: 235–243. doi:10.3354/meps11092

Varpe, Ø. 2012. Fitness and phenology: Annual routines and zooplankton adaptations to seasonal cycles. J. Plankton Res. **34**: 267–276. doi:10.1093/plankt/fbr108

Varpe, Ø., M. Daase, and T. Kristiansen. 2015. A fish-eye view on the new Arctic lightscape. ICES J. Mar. Sci. **72**: 2532–2538. doi:10.1093/icesjms/fsv129

Vestheim, H. 2004. State-dependent vertical distribution of the carnivore copepod *Pareuchaeta norvegica*. J. Plankton Res. **27**: 19–26. doi:10.1093/plankt/fbh144

Vilgrain, L., F. Maps, M. Picheral, M. Babin, C. Aubry, J. Irisson, and S. Ayata. 2021. Trait-based approach using in

situ copepod images reveals contrasting ecological patterns across an Arctic ice melt zone. Limnol. Oceanogr. **66**: 1155–1167. doi:10.1002/lno.11672

Wassmann, P., D. Slagstad, and I. Ellingsen. 2019. Advection of Mesozooplankton into the Northern Svalbard shelf region. Front. Mar. Sci. **6**: 458. doi:10.3389/fmars.2019.00458

Wathne, I., K. Enberg, K. H. Jensen, and M. Heino. 2020. Rapid life-history evolution in a wild *Daphnia pulex* population in response to novel size-dependent predation. Evol. Ecol. **34**: 257–271. doi:10.1007/s10682-020-10031-7

Wood, S. N. 2017. Generalized additive models: An introduction with R, 2nd ed. Chapman and Hall/CRC.

Yen, J. 1985. Selective predation by the carnivorous marine copepod *Euchaeta elongata*: Laboratory measurements of predation rates verified by field observations of temporal and spatial feeding patterns. Limnol. Oceanogr. **30**: 577–597. doi:10.4319/lo.1985.30.3.0577

Zuur, A. F., E. N. Ieno, N. Walker, A. A. Saveliev, and G. M. Smith. 2009. Mixed effects models and extensions in ecology with R. Springer.

Zuur, A. F., E. N. Ieno, and C. S. Elphick. 2010. A protocol for data exploration to avoid common statistical problems. Methods Ecol. Evol. **1**: 3–14. doi:10.1111/j.2041-210X.2009.00001.x

Acknowledgments

T.J.L., J.M.A., and Ø.V. received funding from the Research Council of Norway through the Nansen Legacy project (RCN #276730). J.J.F. was supported by BIOPOLE National Capability Multicentre Round 2 funding from the Natural Environment Research Council (NE/W004933/1). The authors are grateful to all those that helped collect the data during the ecosystem surveys at the Institute of Marine Research. T.J.L thanks the Ecosystems Team at the British Antarctic Survey for hosting him during the writing phase of this project.

Conflict of Interest

None declared.

Submitted 16 September 2022
Revised 08 January 2023
Accepted 05 February 2023

Associate editor: Thomas Kiørboe